SCIENTIFIC REPORTS

OPEN

SUBJECT AREAS:
CHEMICAL BIOLOGY
BIOCHEMISTRY

Received
15 September 2014

Accepted
31 December 2014

Published
27 January 2015

Correspondence and requests for materials should be addressed to P.L. (lograsso@scripps.edu)

Structural Basis and Biological Consequences for JNK2/3 Isoform Selective Aminopyrazoles

HaJeung Park, Sarah Iqbal, Pamela Hernandez, Rudy Mora, Ke Zheng, Yangbo Feng & Philip LoGrasso

Department of Molecular Therapeutics and Translational Research Institute, The Scripps Research Institute, 130 Scripps Way #2A2, Jupiter, Florida 33458.

Three JNK isoforms, JNK1, JNK2, and JNK3 have been reported and unique biological function has been ascribed to each. It is unknown if selective inhibition of these isoforms would confer therapeutic or safety benefit. To probe JNK isoform function we designed JNK2/3 inhibitors that have >30-fold selectivity over JNK1. Utilizing site-directed mutagenesis and x-ray crystallography we identified L144 in JNK3 as a key residue for selectivity. To test whether JNK2/3 selective inhibitors protect human dopaminergic neurons against neurotoxin-induced mitochondrial dysfunction, we monitored reactive oxygen species (ROS) generation and mitochondrial membrane potential (MMP). The results showed that JNK2/3 selective inhibitors protected against 6-hydroxydopamine-induced ROS generation and MMP depolarization. These results suggest that it was possible to develop JNK2/3 selective inhibitors and that residues in hydrophobic pocket I were responsible for selectivity. Moreover, the findings also suggest that inhibition of JNK2/3 likely contributed to protecting mitochondrial function and prevented ultimate cell death.

The c-jun NH_2-terminal kinases (JNKs) are members of the mitogen-activated protein (MAP) kinase family, a group of serine/threonine kinases receiving interest over the past two decades as compelling evidence has implicated them in many diseases such as Parkinson's disease (PD)[1–6], Alzheimer's disease (AD)[7–9], diabetes[10–12], and cardiovascular disease[13–16]. Because of this, numerous medicinal chemistry efforts have been initiated and selective JNK inhibitors have begun to emerge and include compounds from classes such as indazoles[17,18], aminopyrazoles[18], aminopyridines[19,20], pyridine carboxamides[20,21], benzothien-2-yl-amides and benzothiazol-2-yl acetonitriles[22,23], quinoline derivatives[24], and aminopyrimidines[25–27]. For a review of all these classes see LoGrasso and Kamenecka[28]. All of these compounds classes, with the exception of the indazoles, have shown selectivity for JNK over p38, but few have demonstrated selectivity between the three JNK isoforms.

The JNK subfamily is composed of three distinct genes, *jnk1*, *jnk2* and *jnk3*, whose protein products are further subdivided into ten splice variants[29]. JNK3 is primarily expressed in the brain, heart, and pancreas, while JNK 1 and 2 are expressed ubiquitously[30,31]. A series of reports that detail the protective effects of either *jnk3* or *jnk2/3* deletions confer in mice have piqued our interest in developing JNK 2/3 isoform selective inhibitors. In these studies knockout mice possessed resistance to excitotoxic pathways including kainic acid induced seizure[32] and neuronal apoptosis via 1-methyl-4-phenyl-1,2,3,6-tetrahydropyridine (MPTP), a common tool utilized to mimic Parkinson's disease related damage[33]. In addition, neuronal cells from JNK3 knockout mice also have resistance to Aβ-induced apoptosis, the characteristic lesion of Alzheimer's disease[34] and deletion of *jnk3* from familial Alzheimer's disease (FAD) mice resulted in dramatic reduction of Aβ42 levels and overall plaque load[9]. Finally, in support of all of these findings, Fernandes *et al.* reported that *jnk2/3* deletion protected retinal ganglion cells (RGC) in mice from optic nerve crush injury[35]. Collectively, these data are powerful indicators that selective JNK 2/3 inhibitors may have clinical benefit in a variety of neurodegenerative disorders such as PD, AD, and retinal degeneration.

Difficulty of designing selective JNK 2/3 inhibitors is due to high sequence identity among the JNK isoforms. JNK3 shares a 75% amino acid identity with JNK1, and JNK2 shares 73% identity with JNK1. JNK2 and JNK3 are 77% identical at the amino acid level. More importantly, the sequence identity of these enzymes in the ATP binding pocket reaches 98%. In contrast, the amino acid identity for the overall protein and ATP binding pockets between JNK3 and p38 is 48% and 80% respectively. Structural comparison of the C-terminal and N-terminal lobes between JNK3 and JNK1 shows a root-mean square deviation (rmsd) of 1.49 Å and 1.05 Å respectively, while the same comparison between JNK3 and p38 shows 1.69 Å and 1.29 Å respectively. Despite the high level of

amino acid identity between JNK3 and JNK1 and p38, and the three-dimensional structural similarity among these enzymes, it is still possible to make JNK3 isoform selective inhibitors. Indeed, AMG-548, Amgen's former p38 clinical compound, showed a 188-fold selectivity for JNK3 (61 nM) compared to JNK1 (11,480 nM)[36] and a 294-fold selectivity for JNK2 (39 nM) compared to JNK1[36]. In 2009, we reported a class of aminopyrazoles that were highly selective for JNK3 over p38, and also showed modest selectivity (>25-fold) for JNK3 over JNK1[18]. The molecular basis for this isoform selectivity remains unknown. To date no selectivity has been shown for any compound between JNK2 and JNK3.

The current study was designed to understand the molecular basis for JNK2/3 isoform selectivity. To do this we employed structure-based drug design coupled to site-directed mutagenesis to elucidate what residues within JNK3 and JNK1 were crucial for inhibitor selectivity. In addition, we measured the effects of JNK2/3 selective inhibitors in cell-based assays on functional endpoints such as mitochondrial ROS generation and mitochondrial membrane potential to assess the role for JNK isoform contributions to those parameters. The key findings of this work were: 1) Aminopyrazole inhibitors with approximately 30-fold selectivity for JNK3 over JNK1 were designed; 2) Leucine 144 within JNK3, a residue in the hydrophobic I pocket of JNK3, was largely responsible for the selectivity; 3) Inhibition of JNK2/3 may be sufficient to inhibit increases in ROS and decreases in mitochondrial membrane potential in SHSY5Y dopaminergic cells caused by 6-OHDA. These results suggest that selectively targeting JNK2/3 may be effective for preventing JNK-driven mitochondrial dysfunction and cell death.

Results

To understand what molecular features in JNK3 might help confer selectivity of the aminopyrazole class of inhibitors over JNK1 we first simply performed a primary sequence alignment of JNK3α1 with JNK1α1 (Figure 1). Figure 1 presents the partial sequence alignment between JNK3α1 and JNK1α1 for regions that contain residues within the ATP binding pocket. For the 147 amino acids that are displayed in Figure 1, only five (3.4%) differ between JNK3α1 and JNK1α1. From those 147 residues, 23 residues (highlighted with a black square) were within 4 Å of the inhibitor. The five green highlighted residues were ones that differ between the two isoforms in the ATP pocket. Of those, only Leu144 (boxed in red) in JNK3 (Ile106 in JNK1) is within 4 Å of the inhibitor. Furthermore, inspection of the crystal structure showed that L144 forms part of hydrophobic I pocket of JNK3 together with I92, K93, M115, I124, L126, M146, and L206 (Figure 2). Importantly, we also compared similar crystal structures of JNK3[37] and JNK1[38] (each had AMPPNP bound) to see if any of the 23 residues within 4 Å of the inhibitor, despite not being different, might have contributions that affected inhibitor binding. This analysis revealed that the rmsd between JNK3 and JNK1 for these 23 residues was 0.43 Å suggesting nearly identical structure for these residues in the two isoforms. Given the identity of all these residues and the <0.5 Å difference in structure between JNK3 and JNK1 for these key 23 residues, we reasoned that para-substitution on the phenyl ring might be tolerated by the L144 in JNK3 but not the Ile residue found in JNK1. Hence, we chose L144 for mutagenesis.

Table 1 presents the structures for five aminopyrazoles and biochemical IC_{50} values versus WT JNK3, JNK3 L144I, WT JNK1, WT JNK2, and p38. All five inhibitors were modestly potent ATP-competitive inhibitors of WT JNK3 with biochemical IC_{50} values in the range of 35–514 nM. 2-chloro substitution (SR-11165) on the phenyl ring had a minor effect (3.3-fold) of decreasing potency compared to the des-chloro analog (SR-12326). Similarly, para-fluoro phenyl substitution (SR-12327) also had a minor (2.9-fold) potency decreasing effect when compared with the SR-12326. Larger substitutions such as para-chloro phenyl (SR-12103) or para-methyl phenyl (SR-12130) had more dramatic effects decreasing the potency by 14.7-fold and 9.9-fold, respectively when compared to SR-12326. When JNK3 Leu144 was replaced by Ile, the corresponding residue found in JNK1, the IC_{50} values for four of the five compounds increased between 22-fold and >86-fold (Table 1) when compared to WT JNK3. Only the para-chloro phenyl (SR-12103) substitution had a more modest increase of only 4.2-fold. Similarly, the IC_{50} values for WT JNK1 for four of the five compounds increased between 11-fold and >29-fold (Table 1) when compared to WT JNK3. All five inhibitors showed no inhibition for p38 up to 10 μM (Table 1). The IC_{50} values for all five compounds for WT JNK2 (which also has Leu at position 106 in JNK2) were within 4-fold of WT JNK3 (Table 1). Finally, the K_m value of ATP for JNK3 L144I was determined and found to be 2.9 μM, which was nearly identical to the reported value for WT JNK3[39]. Given the ATP competitive nature of these inhibitors it was important that ATP K_m changes, if any, for the mutant were not affecting the binding of the inhibitors.

To understand the structural features within JNK3 and within the aminopyrazoles that were responsible for the JNK3 selectivity we solved the crystal structures for SR-11165, SR-12326, SR-12327, and SR-12130 with WT JNK3 at 2.01 Å, 1.9 Å, 2.65 Å and 2.3 Å, respectively (Supplemental Table 1). Final R_{work}/R_{free} refinements and other refinement statistics are presented in Supplemental Table 1. The overall structure of WT JNK3 with SR-11165 bound is presented in Figure 2A and the stereo view of 2Fo-Fc electron density is presented in Supplemental Figure 1. SR-11165 (shown as a stick model in orange) bound in the ATP pocket (shown as a surface model) where the hydrophobic residues are highlighted in yellow and the polar residues highlighted in cyan. The key L144 residue is highlighted in red and its side chain is shown (Figure 2A). One interesting feature for this binding mode was that the Gly-rich loop folded down

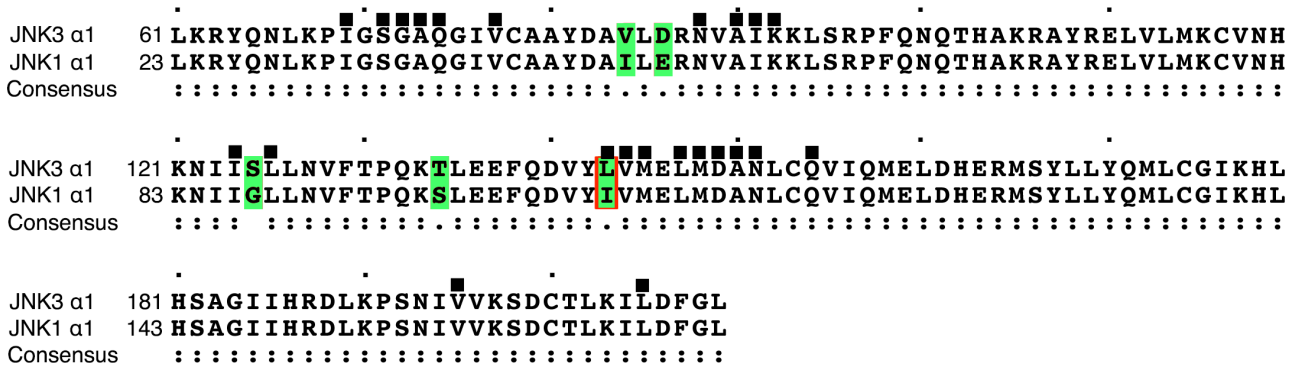

Figure 1 | Partial sequence alignment of JNK3α1 (61–210) and JNK1α1 (23–172) for the region that contains residues within the ATP binding pocket. Residues within the ATP binding pocket are designated by squares. The residues divergent between JNK1 and JNK3 are shaded in green. Residue L144 in JNK3 (or I106 in JNK1) is the only divergent residue that is in the ATP binding pocket.

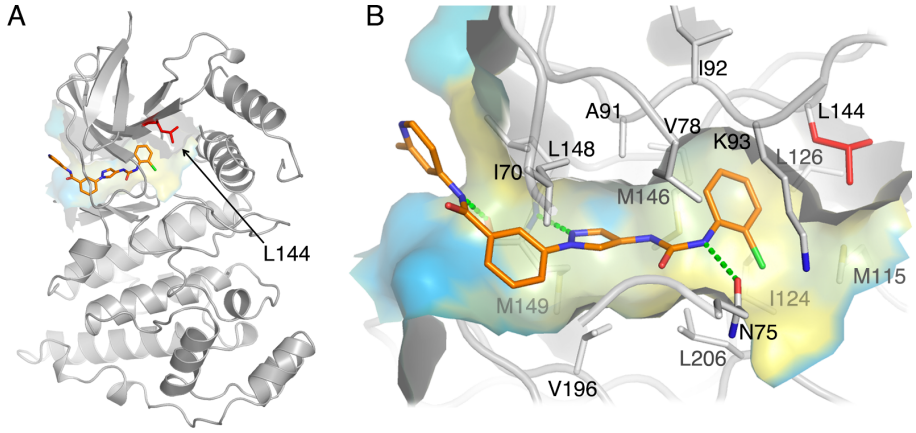

Figure 2 | Crystal structure of JNK3 39–402 and SR-11165 complex. (A) Ribbon diagram showing the overall structure of the complex. SR-11165 in orange and L144 in red are highlighted in stick models. The ATP binding pocket where SR-11165 was bound, is shown as a surface model. The hydrophobic residues and the polar residues are colored in yellow and cyan, respectively. (B) Detailed view of ligand binding pose in the ATP binding pocket of JNK3. The key residues that directly interact with SR-11165 are shown as sticks. Hydrogen bonds are shown as green dash lines. Panels A and B are shown in same orientation and color scheme.

on top of the compound and did not maintain the beta sheet structure more commonly seen with other ligands. It should be noted that all of the compounds used in this study except SR-12326 had the Gly-rich loop folded down. It is inconclusive whether the folded down Gly-rich loop positively influenced inhibitor binding but given the unique observation it was worth noting. Figure 2B shows a detailed view of SR-11165 highlighting all residues of JNK3 within 3.5 Å that have van der Waals interactions with the compound. Key hydrogen bond interactions are shown as dashed green lines and the L144 side chain is indicated in red.

We next superimposed the crystal structures of four of these compounds and a computational model of SR-12103 to see what structural features of the inhibitors and JNK3 were crucial for selectivity and the potency differences that were observed. Figure 3A presents the overlay poses for five JNK3 selective aminopyrazole inhibitors. The Cα RMSD of 351 residues that are superimposed were between 0.16 and 0.24 Å indicating the highly similar structures for all compounds. Optimum binding of inhibitors in the JNK3 pocket were assessed in terms of distances, d1 and d2, which were the distance between C5 position on the phenyl ring of the inhibitors and Cα of

Table 1 | Structures and Biochemical Inhibition for JNK3, JNK3L144I, JNK1, JNK2, and p38 for Various Aminopyrazoles

Structure	Code	JNK3 (IC_{50}, nM)	JNK3L144I (IC_{50}, nM)	JNK1 (IC_{50}, nM)	JNK2 (IC_{50}, nM)	p38 (IC_{50}, nM)
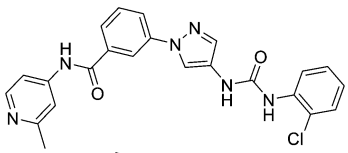	SR-11165	115 ± 16.1	>10,000	2740 ± 280	486 ± 281	NI
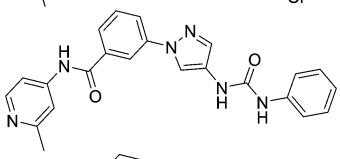	SR-12326	34.7 ± 7.7	1300 ± 443	1013 ± 139	132 ± 93	NI
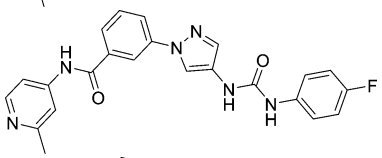	SR-12327	102.8 ± 41.2	2043 ± 449	1147 ± 310	133 ± 94	NI
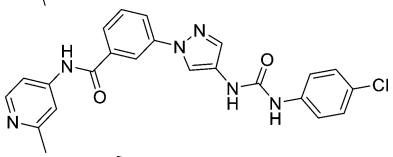	SR-12103	513.7 ± 103.5	2174 ± 693	1506 ± 214	650 ± 460	NI
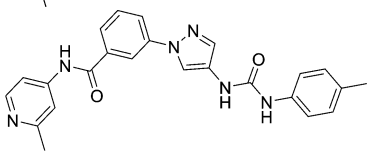	SR-12130	344.8 ± 207.6	>10,000	>10,000	836 ± 591	NI

The biochemical IC_{50} values ± standard error of the mean are the average of ≥3 experiments each performed in triplicate. All enzymes used were human recombinant enzymes. NI = no inhibition at the highest tested concentration of 10,000 nM.

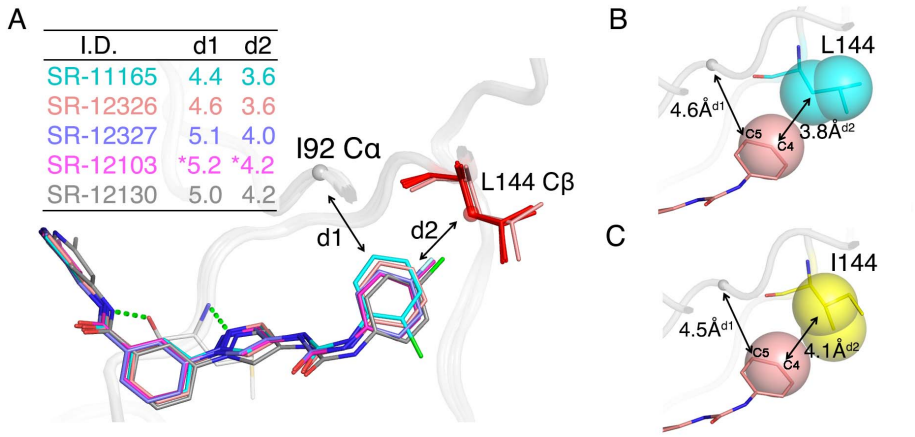

Figure 3 | Overlay poses for five JNK3 selective aminopyrazole inhibitors. (A) A superposition of four crystal structures and one computational model of JNK3 39–402 with aminopyrazole complexes. SR-12103 is a computational model (starred) and the other four complexes were derived from the crystal structures. L144 is colored red for the crystal structures and pink for the model structure. The Cα RMSD of 351 residues that are superimposed was between 0.16 and 0.24 Å. The distances d1 and d2 in the insert table represent distances between C5 of the inhibitor phenyl ring and Cα of I92, and C4 of the inhibitor phenyl ring and Cβ of L144, respectively. (B) The crystal structure of JNK3/SR-12326 was chosen as a representative example for all five compounds bound to JNK3 to illustrate the van der Waals distances differences between Leu 144 and Ile144. The C4 of the phenyl ring of the compound, and Cβ of leucine are shown in Van der Waals spheres, and distances between the carbon atoms are also shown. The optimum distances are predicted with metadynamics calculations. (C) A computational model of SR-12326 bound to JNK3 that is mutated to isoleucine in residue 144 (L144I). The C4 of the phenyl ring of the compound, and Cβ and Cγ of isoleucine are shown in Van der Waals spheres, and distances between the C atoms are also shown.

I92 (d1), and C4 of phenyl ring and Cβ of Leu144 (d2). Substitution on the para position of the inhibitors caused the two distances to increase resulting in the decreased potency of these compounds compared to the para-unsubstituted analog (SR-12326 shown in orange). The van der Waals distances between d1 and d2 for JNK3 which has Leu at position 144 are shown in Figure 3B where the van

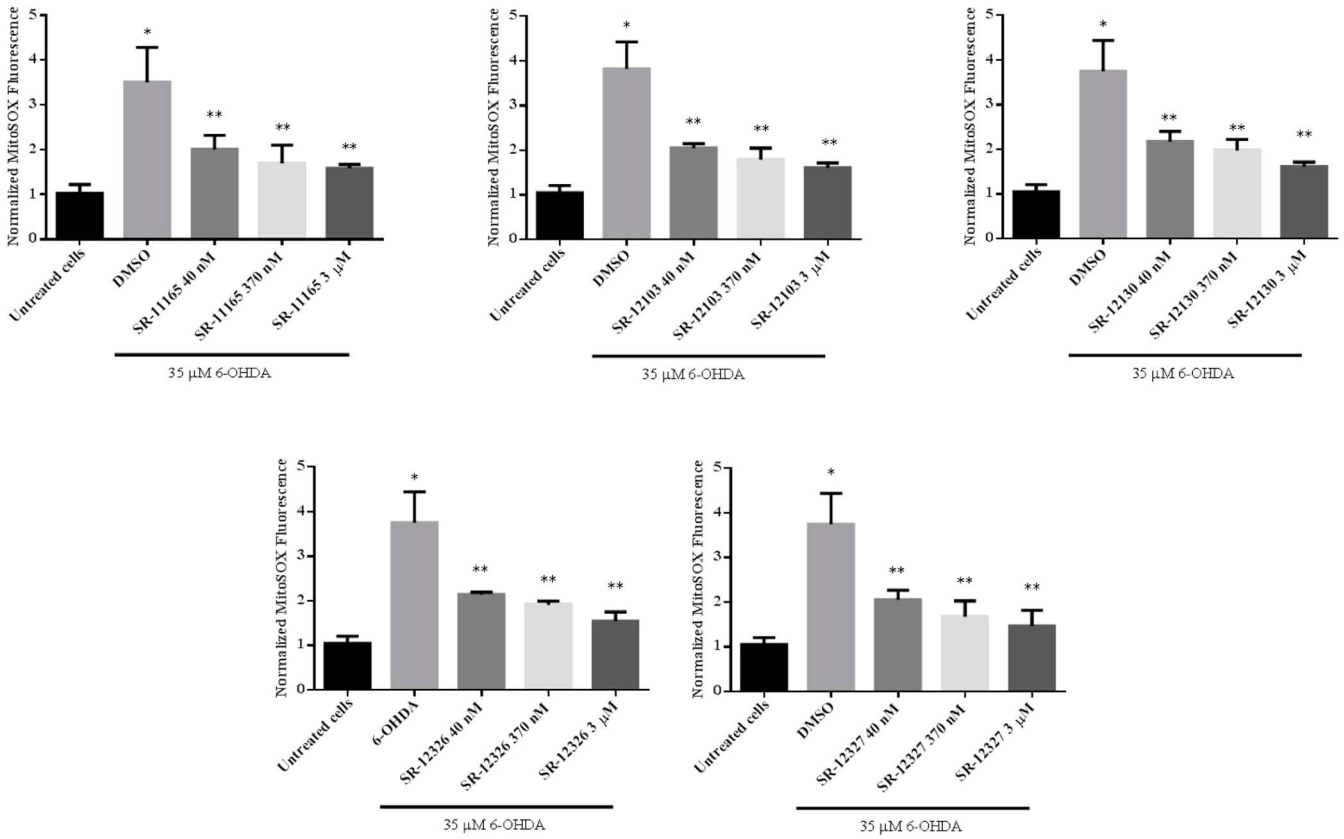

Figure 4 | Inhibition of mitochondrial ROS generation by the JNK2/3 selective aminopyrazole inhibitors in SHSY5Y cells. SHSY5Y cells were treated with 35 μM 6-OHDA for 5 h and mitochondrial ROS was measured by normalized MitoSOX™ fluorescence in the presence or absence of 40, 370 nM and 3 μM of the inhibitors. Statistical significance ($p < 0.05$, ANOVA) between control, untreated group and 6-OHDA treated group is shown by *. Significance ($p < 0.05$, ANOVA) between 6-OHDA-treated groups and different concentrations of the JNK3 selective inhibitors and 6-OHDA-treated groups is shown by * *.

Table 2 | Inhibition of c-Jun phosphorylation and 6-OHDA-induced Mitochondrial Membrane Potential Dissipation in SHSY5Y cells by five JNK2/3 isoform selective inhibitors

Compound ID	p-c-Jun Inhibition IC_{50} ± standard error (nM)		Inhibition of 6-OHDA induced Mitochondrial membrane depolarization IC_{50} ± standard error (nM)	
SR-11165	866 ± 204	n = 5	26 ± 19	n = 2
SR-12326	6638 ± 1158	n = 2	25 ± 10	n = 2
SR-12327	>10,000	n = 2	57 ± 48	n = 2
SR-12103	3440 ± 2216	n = 2	46 ± 29	n = 2
SR-12130	3034 ± 1083	n = 2	42 ± 31	n = 2

der Waals spheres for the phenyl ring in SR-12326 and JNK3 L144 are also shown. For comparison, a computational model of SR-12326 as a representative example of all five compounds bound to JNK3 where Leu was mutated to Ile (L144I) is also shown (Figure 3C). The increased distance (d2) from 3.6 Å (Figure 3B) to 4.0 Å (Figure 3C) for C4 of the phenyl ring of SR-12326 to Cβ and Cγ of isoleucine is indicated. It should be noted that the lowest energy rotameric state of the Ile side chain in the computational model shown in Figure 3C corresponded to the same state determined in the crystal structure for JNK3L144I (Supplemental Figure 2).

After establishing the molecular features within JNK3 and the compounds that were responsible for the potency and isoform selectivity we next wanted to see if isoform selective inhibitors still maintained their potency *in vitro* for inhibition of 6-OHDA-induced c-Jun phosphorylation and attenuation of mitochondrial ROS generation and mitochondrial membrane potential (MMP) depolarization. We previously established that a class of aminopyrimidines were potent pan JNK inhibitors that also potently inhibited c-Jun phosphorylation, reactive oxygen species generation, and MMP dissipation in many cell types including cardiomyocytes, INS-1 pancreatic β-cells, and primary dopaminergic neurons[1,2,14,27].

Here we were able to assess whether inhibition of all three JNK isoforms were needed to inhibit c-Jun phosphorylation, mitochondrial ROS, and MMP dissipation and assess what the contribution for JNK1 would be to each of these functions. Table 2 presents the cell-based inhibition of 6-OHDA-induced-c-Jun phosphorylation and MMP depolarization in SHSY5Y cells. Four of the five compounds had EC_{50} values for inhibition of c-Jun phosphorylation >3 μM, with SR-12327 having an EC_{50} value > 10 μM. Only SR-11165 had an EC_{50} value < 1 μM (Table 2). Despite the weak inhibition of c-Jun phosphorylation all five compounds had EC_{50} values between 25–57 nM range for the inhibition of 6-OHDA-induced MMP depolarization (Table 2). Importantly, a structural analog of SR-11165, SR-11404 (Supplemental Figure 3), which was designed to have no inhibition against JNKs 1-3 because of a methyl group on the hinge binding amide, showed no inhibition of 6-OHDA-induced MMP depolarization. To corroborate the MMP findings we also measured the inhibition of mitochondrial ROS generation by JNK2/3 selective inhibitors in SHSY5Y cells. Figure 4 presents the normalized MitoSOX fluorescence for the five compounds presented in Table 1. All five compounds showed potent inhibition of mitochondrial ROS at concentrations between 40 nM and 3 μM consistent with the MMP findings.

Discussion

We previously reported a class of aminopyrazoles that showed >2800-fold selectivity for JNK3 over p38 and 25-fold selectivity over JNK1[18]. The selectivity over p38 was largely described by the planar nature of the pyrazoles as well as the smaller active site in JNK3 as compared to p38. That study however did not investigate the reason for the selectivity of these compounds for JNK3 over JNK1. In addition, the functional consequences of this selectivity were not examined in a biological system. In this report we utilized site directed mutagenesis and x-ray crystallography to show that L144 in JNK3, which corresponds to Ile106 in JNK1 was largely responsible for the JNK3 selectivity in this class of inhibitors. In addition, we also investigated the biological effects of JNK2/3 inhibition in neuronal cells.

The mutagenesis results showed that Leu144 in hydrophobic pocket I was the key structural feature within JNK3 that gave rise to the selectivity of the aminopyrazoles for JNK3 over JNK1. The greater than 22-fold increase in IC_{50} value for four of the five compounds tested in this study upon mutagenesis of Leu144 to Ile supports this conclusion as does the shift of L144I mutant IC_{50} values in the range for that of WT JNK1. In an attempt to understand why this class had such selectivity we overlayed the crystal structure of SR-12326 with that of compound 9l (SR-3562) from our previously reported aminopyrimidine class of pan JNK inhibitors[27] (Figure 5). The overlay showed that the phenyl ring of SR-12326 projected into hydrophobic pocket I where the aminopyrimidines represented by SR-3562 did not. Thus, it is likely that the interaction of the hydrophobic pocket residues with the phenyl ring of SR-12326 was largely responsible for the selectivity of this class for JNK3 over JNK1. Indeed, any class of compounds that exploits this pocket, and in particular the Leu144 residue, is likely to demonstrate high selectivity for JNK3 over JNK1. This conclusion is supported by the findings of Swahn *et al.* who in 2006 reported the only other known JNK3 isoform selective class of inhibitors[19]. Like the aminopyrazoles presented in this work, the anilino-bipyridines reported by Swahn *et al.* showed 55-fold selectivity for JNK3 over JNK1. Furthermore the crystal structure for one of their compounds showed that the pyridyl group was in hydrophobic pocket I of JNK3 having contacts with Leu144. It is important to note that while the anilino-bipyridines reported by Swahn *et al.*[19] had selectivity for JNK3 over JNK1 in the same magnitude range as our compounds, they did not have high selectivity over p38 thereby making them unsuitable for biological

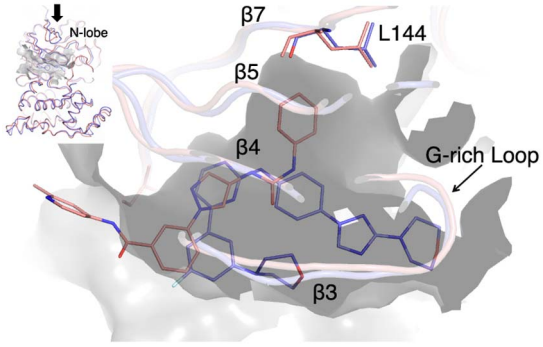

Figure 5 | Overlay of complex crystal structures of JNK3:SR-12326 (pink) and JNK3:SR-3562 (blue, PDB ID: 3KVX). The inhibitor binding modes between SR-12326 and SR-3562, an aminopyrzaole and an aminopyrimidine, respectively are compared. The SR-3562 binding site of JNK3 is located under the β-strands β3/4 and G-rich loop, whereas the SR-12326 binding site was located deeper into the pocket under N-lobe β-sheet β3/4/5/7. The arrow in the insert figure indicates viewing direction in the main figure. The inhibitor binding pocket of JNK3 in JNK3:SR-12326 complex is shown as a grey surface.

evaluation in cell-based assays to assess the role of JNK in mitochondrial function and cell death. Moreover, no cell-based inhibition data was reported so it is unclear if these compounds were cell permeable or potent *in vitro* JNK inhibitors.

The SAR for the compounds presented in Table 1 can best be understood by comparison of the interactions for each compound. Para-substitution on the phenyl ring was accommodated by Leu144 in JNK3 because the phenyl ring was shifted further away from the hydrophobic pocket I as evidenced by the increased distance (d1) from the Cα of Ile92, a component of the hydrophobic pocket I. Moreover, substitution at the para-position caused the van der Waals interaction to increase at d1 and d2 thereby slightly decreasing the potency. Furthermore, making the Ile144 substitution increased the van der Waals distance between Ile144 Cβ and Cγ compared to Leu thereby making compounds less potent for mutant even though SR-12326 was unsubstituted.

While the structural features of the enzyme and inhibitors can help explain the isoform selectivity, it required *in vitro* cell-based assays to help assess the contribution that JNK3 and JNK2 make towards mitochondrial dysfunction. Since all three JNK isoforms phosphorylate c-Jun, the most likely explanation for why four of the five compounds had IC_{50} values > 3 μM (and the fifth was near 1 μM) was that despite modestly potent JNK3 and JNK2 inhibition, JNK1 was not potently inhibited in the cells due to the isoform selectivity of these compounds and as such the JNK1 activity was likely responsible for the c-Jun phosphorylation. Indeed, the cell-based IC_{50} values were in a similar range as the JNK1 biochemical IC_{50} values (Tables 1 and 2). Poor cell permeability for these compounds cannot be ruled out, but this is highly unlikely as these compounds were potent inhibitors of mitochondrial ROS generation and MMP dissipation (Table 2, Figure 4).

The findings for the MMP dissipation and inhibition of mitochondrial ROS generation can best be explained by the fact that unlike c-Jun phosphorylation, MMP dissipation and mitochondrial ROS generation may not have a significant contribution from JNK1 and that this parameter is largely a function of JNK3 and JNK2 activity. Indeed, the results seen in the current study were similar to our findings for the aminopyrimidines where the IC_{50} value for inhibition of ROS generated by the mitochondria was approximately 1 nM and the inhibition of c-Jun phosphorylation was 50 nM for SR-3562. It may be that only a small amount of JNK3 and JNK2 inhibition goes a long way towards shutting down JNK mitochondrial function. This interpretation is consistent with the *in vivo* observations of Zhao and Herdegen who reported that basal physiological JNK1 activity is replaced in mitochondria by activated JNK3 and JNK2 following neurodegenerative events[40]. Moreover, this possibility is further supported by the findings of Davis and colleagues who showed that TNFα-induced ROS production was JNK-dependent, and that almost no ROS production, as measured by CM-H_2DCFDA detection, was seen in *jnk*-/- fibroblasts[41]. Similar findings were reported by Karin and colleagues who also showed that TNFα-induced ROS production had a significant JNK dependence[42]. Further confirmation of this explanation could be achieved with a JNK1 selective (over JNK3 and JNK2) inhibitor as it would be expected that such a compound would not greatly affect mitochondrial ROS generation or MMP depolarization. Thus far we have not designed such a molecule. However, the lack of inhibition for MMP depolarization by SR-11404, the inactive structural analog of SR-11165 lends further support that JNK3 and JNK2 inhibition contributed significantly to ROS generation and MMP dissipation. It cannot be ruled out that off-target kinase effects of the aminopyrazoles could also contribute to the increased potency of MMP dissipation, but this interpretation is unlikely given that at 10 μM only 2.2% of the 447 kinases tested with an analog of those reported showed any binding at all in an Ambit screen[43]. Finally, we cannot rule out alternative interpretations such as other signaling pathways that do not have a kinase component contributing to ROS or MMP changes in the mitochondria so this remains a possibility for the greater potency in ROS generation and MMP dissipation for these compounds.

This is the first report for a structural class of compounds that shows high selectivity for JNK3 over JNK1 and p38. Through a series of mutagenesis, SAR, and structural studies we showed that Leu144 in JNK3 and regions of the hydrophobic pocket I were essential to accommodate side chains from the aminopyrazoles class and that fine interactions between Leu144, Ile92, and para-substitutions of the phenyl ring can have effects on the potency of these compounds. Finally, our results suggest that inhibition of JNK3 and JNK2 may be suitable to achieve high degrees of inhibition of mitochondrial dysfunction. This observation may have great significance if it is ever proven that full efficacy can be achieved solely by inhibiting JNK mitochondrial function, if pan JNK inhibition has untoward side effects in man, or if it is shown that inhibition of JNK nuclear signaling is either not needed for efficacy in protecting neurons, or if inhibition of nuclear signaling proves to have an unsuitable toxicity profile. Indeed, many studies report the importance of JNK3 and JNK2, especially in neurodegenerative disease, so isoform selective inhibitors may be a great pharmacological tool and potentially a great therapeutic avenue to probe these findings.

Methods

Expression and Purification of JNK3, JNK3L144I, and ATF2. WT JNK3 and ATF2 were expressed and purified as previously described[18]. Site directed mutagenesis of Leu144 to Ile was done using polymerase chain reaction with primer sets, 5′GGAGTTCCAAGATGTTTACATCGTAATGGAACTGATGGATGC3′ and 5′GCATCCATCAGTTCCATTACGATGTAAACATCTTGGAACTCC3′, and the template vector pET15b-JNK3 39-402. The L144I mutation was confirmed by DNA sequencing. Expression of JNK3 L144I was accomplished in the same manner as WT JNK3.

***in vitro* activation of WT JNK3 and JNK3 L144I.** WT JNK3 39–402 and JNK3 39–402 L144I were activated with upstream kinases MKK4 and MKK7, which were purchased from Millipore. 300 nM of JNK3 proteins in 200 μL volume were incubated for 2 h at 30°C with 100 nM each of MKK4 and MKK7 in kinase reaction buffer containing 25 mM HEPES (pH 7.5), 10 mM $MgCl_2$, 2 mM DTT, 1 mM β-pyrophosphate and 200 μM ATP. The phosphorylation state of the activated JNK3 proteins was confirmed by mass spectrometry analysis, Western analysis using p-JNK antibody, (Cell Signaling) and specific activity assays.

Homogeneous Time-resolved Flourescence Assay (HTRF) for IC_{50} determination. Enzyme inhibition assays were performed as described[18] with minor modifications as noted below. The reaction was run for one hour using 0.5 μM biotinylated FL-ATF-2, 1.25 μM ATP, 0.75 nM activated WT JNK3α1, JNK3α1L144I, or WT JNK1 (purchased from Millipore). p38 enzyme inhibition assays were performed as previously reported[18].

Cell-based Assays Measuring JNK Activity. SHSY5Y cells (ATCC) were grown at 37°C and 5% CO2 in DMEM/F:12 (Invitrogen) supplemented with 10% fetal bovine serum and penicillin/streptomycin. To assure that the cells were actively growing, only cells at ~80% confluency and between passages five and fifteen were used in our experiments. The In cell Western assay was performed as follows: 60,000 SHSY5Y cells/well were plated in a clear-bottomed Packard View black 96-well plate (Millipore) in 100 μl of 10% FBS DMEM:F12 medium and allowed to attach overnight. The next day, cells were treated with the inhibitors (15 nM-10,000 nM) for 1 h prior to induction of JNK pathway activation with 35 μM 6-hydroxydopamine (6-OHDA) for 4–5 h. Cells were fixed in 4% paraformaldehyde in PBS for 20 min at RT with no shaking and were washed once with 0.1 M glycine to neutralize paraformaldehyde for 5 min under gentle shaking. Next, cells were permeated with 0.2% Triton X-100 in PBS for 20 min at RT on an orbital shaker and washed once with PBS for 5 min and blocked with Licor Blocking Buffer in PBS (1 : 1 dilution in PBS) for 1–1.5 h rocking at RT. Cells were incubated with the primary antibody (pcJun S63 Ab (Cell Signaling # 9261) 1 : 100 dilution in Licor blocking buffer) overnight at 4°C with rocking. The next day, cells were washed twice with PBS-0.1% Tween 20 (PBST) washing solution 5 min each at room temperature on the orbital shaker. Next, cells were washed once with Licor Blocking Buffer containing 0.05% Tween-20 for 5 min at RT on a shaker. Cells were incubated with secondary antibody (goat anti-rabbit IR800 1 : 500 dilution) in Licor blocking buffer + Tween-20 for 1 h rocking at RT in the dark. After that the cells were washed twice with PBST for 5 min each at RT, and then washed once with Licor blocking buffer containing 0.05% Tween-20 and incubated with ToPro 3 (nucleic acid staining) diluted 1 : 4000 in Licor blocking buffer or Licor blocking buffer with 0.05% Tween-20 for 30 min at RT in the dark. Prior to analysis cells were washed twice with PBS and analyzed using the Odyssey LICOR infrared scanner.

Mitochondrial membrane depolarization. 60,000 SHSY5Y cells/well were seeded into black-walled, clear-bottomed 96-well plates (Millipore). Cells were incubated with inhibitors (15 nM-10,000 nM) for 1 h before adding 35 μM 6-OHDA for 4 h. After a 4 h incubation, cells were stained with 500 nM MitoTracker® Orange CMTRos for 30 minutes under growth conditions to measure mitochondrial membrane depolarization. The cells were washed twice in Hank's Buffer Salt Solution (HBSS), and placed in pre-warmed HBSS for fluorescent recordings. Fluorescence was detected by exciting the fluorophore at 554 nm and monitoring the emission at 576 nm on a SpectraMax e5 plate reader (Molecular Devices). Mitochondrial membrane depolarization was normalized to cell abundance by staining the cells with Hoechst 33342 (excitation: 350 nm; emission: 450 nm).

Mitochondrial Superoxide Production. Mitochondrial superoxide generation was monitored by MitoSOX Red (Invitrogen) fluorescence. SH-SY5Y cells (50,000 cells/well) were seeded in to black walled, clear bottomed 96-well plate. Cells were incubated with inhibitors (40 nM, 370 nM, 3000 nM) for 1 h before adding 35 μM 6-OHDA for 5 h. Cells were stained with 2.5 μM MitoSOX Red for 25 minutes under growth conditions. The cells were washed twice in Hank's Buffer Salt Solution (HBSS), and placed in pre-warmed HBSS for imagining. MitoSOX Red fluorescence was detected by exciting the fluorophore at 510 nm and monitoring the emission at 580 nm on a SpectraMax e5 plate reader (Molecular Devices). Mitochondrial superoxide was normalized to cell abundance by staining the cells with Hoechst 33342 (excitation: 350 nm; emission: 450 nm).

Statistical Analysis for Cell-based Assays. For mitochondrial superoxide detection, and mitochondrial membrane potential, three sample replicates were measured for the three biological replicates obtained for each treatment. All statistics displayed were performed using the ANOVA with Tukey's comparison. A p-value of 0.05 was used to determine significance.

Crystallization of JNK3 and JNK3L144I. The crystals of JNK3 39–402 for ligand soaking experiments were grown using the vapor diffusion method at 4°C using a precipitant containing 0.2 M ammonium tartrate pH 7.0, 20% PEG 3350 and 10 mg/mL of JNK3 pre-incubated with 1 mM ATP on ice. Hanging drop plates with 3 μL drops containing 1 : 1 protein-precipitant mixture and 500 μL of the precipitant were incubated at 4°C. Crystals appeared after 24 h of incubation and grew continuously until the size became approximately 50 × 50 × 100 μm. The soaking solution for each compound was prepared by dilution of 50 mM of compound in 100% DMSO to 2∼5 mM with the precipitant. Full-grown crystals were transferred to the soaking solutions and were incubated 3∼24 h before harvesting for data collection. The crystals were then transferred to mounting loops and excess soaking solutions were removed and flash frozen by plunging into liquid nitrogen.

Data collection and refinement. Diffraction datasets were obtained at beam line 11-1 of SLAC (SSRL), LS-CAT 21-IDG (APS), and at an in-house diffraction facility equipped with a Micromax-007 HFM (Rigaku) and a Mar345dtb (Mar Research). The datasets were processed with autoProc with MOSFLM as the data reduction engine[44,45]. The crystals belonged to $P2_12_12_1$ with the approximate unit cell dimensions $a \approx 53$ Å, $b \approx 71$ Å, and $c \approx 108$ Å with one molecule in the assymetric unit. The unit cell values indicated the crystal packing was the same as PDB ID 1JNK, which is the most fequent crystal form of JNK3 crystals in PDB data base. PDB ID 1JNK was used as the initial refinement model. Quick molecular replacements using Phaser in Phenix suite[46], properly positoned JNK3 and showed free and crystallographic R-factors values around 35%. Bound compounds were clearly identified as positive densities in ATP binding pockets. Restraints and coordintates for the compounds were generated using eLBOW in Phenix suite and incorporated into the JNK3 coordinate using the graphics program Coot[47]. The models were then refined using Buster (Global Phasing Ltd.) with TLS (translation, libration, and screw-motion), water update and unknown ligand search options turned on. The models were manually inspected and adjusted after each refinement cycle using Coot. After six to ten cycles of refinements, the free and crystallographic R-factors stabilized. Data processing and refinement statistics are given in Supplemental Table 1. Structural analysis and figure preparations were done with PyMol (Schrodinger, LLC). PDB i.d. numbers for the four structures are: 4W4V; 4W4W; 4W4X; and 4W4Y.

Computational modeling, metadynamics calculations. For a computational model of JNK3:SR-12103 complex, the H- at phenyl C_4 was substituted with Cl- in co-crystal structure of JNK3:SR-12326 using Maestro (Schrodinger, LLC) followed by Prime energy minimization of the inhibitor and the residues within 5 Å of the inhibitor. A computational model of SR-12326 bound to JNK3 L114I was also produced in Maestro by mutating L144 to Ile followed by the same minimization protocol used for JNK3:SR-12103. The metadynamics calculations were conducted using Schrodinger distribution of Desmond 3.4 (DE Shaw Research) with OPLS_2005 force field. Briefly, the modeled coordinate of JNK3 L144I:SR-12326 and the co-crystal structure of JNK3:SR-12326 were solvated in an orthorhombic box with TIP3 water and 150 mM NaCl which buffer 10 Å each direction. The systems were pre-equilibrated using the NPT relaxation protocol, which consists of restrained followed by unrestrained minimizations and short simulations with isothermal and isobaric ensemble. Production runs were run for 10 ns at constant temperature (300 K) and pressure (1.01325 bar). Short- and long- range Coulombic interactions were set to Cutoff method with 9 Å radius and smooth particle mesh Ewald tolerance method with the tolerance of 1×10^{-9}, respectively. Distances between C5 of the inhibitor phenyl ring and Cα of I92 (d1), and C4 of the inhibitor phenyl ring and Cβ of L144 (d2) were set as collective variables. Two dimensional free energy surfaces for the collective variables were determined at the end of the simulation run.

1. Chambers, J. W., Howard, S. & LoGrasso, P. V. Blocking c-Jun N-terminal kinase (JNK) translocation to the mitochondria prevents 6-hydroxydopamine-induced toxicity in vitro and in vivo. *J Biol Chem* **288**, 1079–1087; DOI:10.1074/jbc.M112.421354 (2013).
2. Chambers, J. W. *et al.* Small Molecule c-jun-N-terminal Kinase (JNK) Inhibitors Protect Dopaminergic Neurons in a Model of Parkinson's Disease. *ACS Chem Neurosci* **2**, 198–206; DOI:10.1021/cn100109k (2011).
3. Crocker, C. E. *et al.* JNK Inhibition Protects Dopamine Neurons and Provides Behavioral Improvement in a Rat 6-Hydroxydopamine Model of Parkinson's Disease. *ACS Chem. Neurosci.* **2**, 207–212; DOI:10.1021/cn1001107 (2011).
4. Feng, Y. *et al.* A small molecule bidentate-binding dual inhibitor probe of the LRRK2 and JNK kinases. *ACS Chem Biol* **8**, 1747–1754; DOI:10.1021/cb3006165 (2013).
5. Hunot, S. *et al.* JNK-mediated induction of cyclooxygenase 2 is required for neurodegeneration in a mouse model of Parkinson's disease. *Proc Natl Acad Sci U S A* **101**, 665–670 (2004).
6. Xia, X. G. *et al.* Gene transfer of the JNK interacting protein-1 protects dopaminergic neurons in the MPTP model of Parkinson's disease. *Proc Natl Acad Sci U S A* **98**, 10433–10438 (2001).
7. Braithwaite, S. P. *et al.* Inhibition of c-Jun kinase provides neuroprotection in a model of Alzheimer's disease. *Neurobiol Dis* **39**, 311–317; DOI:10.1016/j.nbd.2010.04.015 (2010).
8. Pearson, A. G., Byrne, U. T., MacGibbon, G. A., Faull, R. L. & Dragunow, M. Activated c-Jun is present in neurofibrillary tangles in Alzheimer's disease brains. *Neuroscience letters* **398**, 246–250; DOI:10.1016/j.neulet.2006.01.031 (2006).
9. Yoon, S. O. *et al.* JNK3 perpetuates metabolic stress induced by Abeta peptides. *Neuron* **75**, 824–837; DOI:10.1016/j.neuron.2012.06.024 (2012).
10. Bonny, C., Oberson, A., Negri, S., Sauser, C. & Schorderet, D. F. Cell-permeable peptide inhibitors of JNK: novel blockers of beta-cell death. *Diabetes* **50**, 77–82 (2001).
11. Hirosumi, J. *et al.* A central role for JNK in obesity and insulin resistance. *Nature* **420**, 333–336; DOI:10.1038/nature01137 (2002).
12. Kaneto, H. *et al.* Possible novel therapy for diabetes with cell-permeable JNK-inhibitory peptide. *Nat Med* **10**, 1128–1132; DOI:10.1038/nm1111 (2004).
13. Borsello, T. *et al.* A peptide inhibitor of c-Jun N-terminal kinase protects against excitotoxicity and cerebral ischemia. *Nat Med* **9**, 1180–1186 (2003).
14. Chambers, J. W., Pachori, A., Howard, S., Iqbal, S. & LoGrasso, P. V. Inhibition of JNK mitochondrial localization and signaling is protective against ischemia/reperfusion injury in rats. *J Biol Chem* **288**, 4000–4011; DOI:10.1074/jbc.M112.406777 (2013).
15. Kerkela, R. *et al.* Cardiotoxicity of the cancer therapeutic agent imatinib mesylate. *Nat Med* **12**, 908–916; DOI:10.1038/nm1446 (2006).
16. Ferrandi, C. *et al.* Inhibition of c-Jun N-terminal kinase decreases cardiomyocyte apoptosis and infarct size after myocardial ischemia and reperfusion in anaesthetized rats. *Brit J Pharmacol* **142**, 953–960; DOI:10.1038/sj.bjp.0705873 (2004).
17. Swahn, B. M. *et al.* Design and synthesis of 6-anilinoindazoles as selective inhibitors of c-Jun N-terminal kinase-3. *Bioorg Med Chem Lett* **15**, 5095–5099 (2005).
18. Kamenecka, T. *et al.* Structure-activity relationships and X-ray structures describing the selectivity of aminopyrazole inhibitors for c-Jun N-terminal kinase 3 (JNK3) over p38. *J Biol Chem* **284**, 12853–12861; DOI:10.1074/jbc.M809430200 (2009).
19. Swahn, B. M. *et al.* Design and synthesis of 2'-anilino-4,4'-bipyridines as selective inhibitors of c-Jun N-terminal kinase-3. *Bioorg Med Chem Lett* **16**, 1397–1401; DOI:10.1016/j.bmcl.2005.11.039 (2006).
20. Szczepankiewicz, B. G. *et al.* Aminopyridine-based c-Jun N-terminal kinase inhibitors with cellular activity and minimal cross-kinase activity. *J Med Chem* **49**, 3563–3580 (2006).
21. Zhao, H. *et al.* Discovery of potent, highly selective, and orally bioavailable pyridine carboxamide c-Jun NH2-terminal kinase inhibitors. *J Med Chem* **49**, 4455–4458 (2006).
22. Angell, R. M. *et al.* N-(3-Cyano-4,5,6,7-tetrahydro-1-benzothien-2-yl)amides as potent, selective, inhibitors of JNK2 and JNK3. *Bioorg Med Chem Lett* **17**, 1296–1301 (2007).
23. Gaillard, P. *et al.* Design and synthesis of the first generation of novel potent, selective, and in vivo active (benzothiazol-2-yl)acetonitrile inhibitors of the c-Jun N-terminal kinase. *J Med Chem* **48**, 4596–4607 (2005).
24. Jiang, R. *et al.* 3,5-Disubstituted quinolines as novel c-Jun N-terminal kinase inhibitors. *Bioorg Med Chem Lett* **17**, 6378–6382; DOI:10.1016/j.bmcl.2007.08.054 (2007).
25. Alam, M. *et al.* Synthesis and SAR of aminopyrimidines as novel c-Jun N-terminal kinase (JNK) inhibitors. *Bioorg Med Chem Lett* **17**, 3463–3467 (2007).
26. Humphries, P. S. *et al.* Synthesis and SAR of 4-substituted-2-aminopyrimidines as novel c-Jun N-terminal kinase (JNK) inhibitors. *Bioorg Med Chem Lett* **19**, 2099–2102; DOI:10.1016/j.bmcl.2009.03.023 (2009).

27. Kamenecka, T. *et al*. Synthesis, biological evaluation, X-ray structure, and pharmacokinetics of aminopyrimidine c-jun-N-terminal kinase (JNK) inhibitors. *J Med Chem* **53**, 419–431; DOI:10.1021/jm901351f (2010).
28. LoGrasso, P. & Kamenecka, T. Inhibitors of c-jun-N-terminal kinase (JNK). *Mini Rev Med Chem* **8**, 755–766 (2008).
29. Gupta, S. *et al*. Selective interaction of JNK protein kinase isoforms with transcription factors. *Embo Journal* **15**, 2760–2770 (1996).
30. Martin, J. H., Mohit, A. A. & Miller, C. A. Developmental expression in the mouse nervous system of the p49(3F12) SAP kinase. *Mol Brain Res* **35**, 47–57 (1996).
31. Abdelli, S. *et al*. JNK3 is abundant in insulin-secreting cells and protects against cytokine-induced apoptosis. *Diabetologia* **52**, 1871–1880; DOI:10.1007/s00125-009-1431-7 (2009).
32. Yang, D. D. *et al*. Absence of excitotoxicity-induced apoptosis in the hippocampus of mice lacking the Jnk3 gene. *Nature* **389**, 865–870 (1997).
33. Hunot, S. *et al*. JNK-mediated induction of cyclooxygenase 2 is required for neurodegeneration in a mouse model of Parkinson's disease. *PNAS* **101**, 665–670 (2004).
34. Morishima, Y. *et al*. beta-amyloid induces neuronal apoptosis via a mechanism that involves the c-Jun N-terminal kinase pathway and the induction of Fas ligand. *J Neurosci* **21**, 7551–7560 (2001).
35. Fernandes, K. A. *et al*. JNK2 and JNK3 are major regulators of axonal injury-induced retinal ganglion cell death. *Neurobiol Dis* **46**, 393–401; DOI:10.1016/j.nbd.2012.02.003 (2012).
36. Dominguez, C., Powers, D. A. & Tamayo, N. p38 MAP kinase inhibitors: many are made, but few are chosen. *Cur Opin Drug Discovery Dev* **8**, 421–430 (2005).
37. Xie, X. *et al*. Crystal structure of JNK3: a kinase implicated in neuronal apoptosis. *Structure* **6**, 983–991 (1998).
38. Garai, A. *et al*. Specificity of linear motifs that bind to a common mitogen-activated protein kinase docking groove. *Sci Signal* **5**, ra74; DOI:10.1126/scisignal.2003004 (2012).
39. Ember, B., Kamenecka, T. & LoGrasso, P. Kinetic mechanism and inhibitor characterization for c-jun-N-terminal kinase 3alpha1. *Biochemistry* **47**, 3076–3084; DOI:10.1021/bi701852z (2008).
40. Zhao, Y. & Herdegen, T. Cerebral ischemia provokes a profound exchange of activated JNK isoforms in brain mitochondria. *Mol Cellular Neurosci* **41**, 186–195; DOI:10.1016/j.mcn.2009.02.012 (2009).
41. Ventura, J. J., Cogswell, P., Flavell, R. A., Baldwin, A. S., Jr. & Davis, R. J. JNK potentiates TNF-stimulated necrosis by increasing the production of cytotoxic reactive oxygen species. *Genes Dev* **18**, 2905–2915; DOI:10.1101/gad.1223004 (2004).
42. Kamata, H. *et al*. Reactive oxygen species promote TNFalpha-induced death and sustained JNK activation by inhibiting MAP kinase phosphatases. *Cell* **120**, 649–661; DOI:10.1016/j.cell.2004.12.041 (2005).
43. Fabian, M. A. *et al*. A small molecule-kinase interaction map for clinical kinase inhibitors. *Nature Biotech* **23**, 329–336 (2005).
44. Leslie, A. G. The integration of macromolecular diffraction data. *Acta Crystallogr D Biol Crystallogr* **62**, 48–57; DOI:10.1107/S0907444905039107 (2006).
45. Vonrhein, C. *et al*. Data processing and analysis with the autoPROC toolbox. *Acta Crystallogr D Biol Crystallogr* **67**, 293–302; DOI:10.1107/S0907444911007773 (2011).
46. Adams, P. D. *et al*. PHENIX: a comprehensive Python-based system for macromolecular structure solution. *Acta Crystallogr D Biol Crystallogr* **66**, 213–221; DOI:10.1107/S0907444909052925 (2010).
47. Emsley, P. & Cowtan, K. Coot: model-building tools for molecular graphics. *Acta Crystallogr D Biol Crystallogr* **60**, 2126–2132; DOI:10.1107/S0907444904019158 (2004).

Acknowledgments

This work was supported by NIH grant, GM103825 and DOD grant, W81XWH-12-1-0431 awarded to P.L.

Author contributions

H.P., Y.F. and P.L. designed the experiments. H.P., S.I., P.H., R.M. and K.Z. performed the experiments. H.P., S.I., Y.F., K.Z. and P.L. interpreted the data. P.L. wrote the manuscript.

Additional information

Accession codes: PDB i.d. numbers for the four structures are: 4W4V; 4W4W; 4W4X; and 4W4Y.

Supplementary information accompanies this paper at http://www.nature.com/scientificreports

Competing financial interests: Philip LoGrasso serves as a consultant for OPKO Health

How to cite this article: Park, H. *et al*. Structural Basis and Biological Consequences for JNK2/3 Isoform Selective Aminopyrazoles. *Sci. Rep.* **5**, 8047; DOI:10.1038/srep08047 (2015).